

## Optimal Frequency for Microfluidic Mixing across a Fluid Interface

Sanjeeva Balasuriya\*

*School of Mathematical Sciences, University of Adelaide, SA 5005, Australia*

(Received 6 May 2010; revised manuscript received 23 June 2010; published 6 August 2010)

A new analytical tool for determining the optimum frequency for a micromixing strategy to mix two fluids across their interface is presented. The frequency dependence of the flux is characterized in terms of a Fourier transform related to the apparatus geometry. Illustrative microfluidic mixing examples based on electromagnetic forcing and fluid pumping strategies are presented.

DOI: 10.1103/PhysRevLett.105.064501

PACS numbers: 47.61.Ne, 47.10.Fg, 47.52.+j

*Introduction.*—Many micro- and nanofluidic devices require rapid mixing of a sample and a reagent, to enhance reaction rates in biochemical assays. Nevertheless, the inevitable low Reynolds numbers associated with such devices means that turbulent mixing is suppressed. Diffusive time- and length scales for good mixing are also usually impractical, leading to considerable interest in devising strategies to optimize mixing. Active (energy-supplying) techniques used range from mechanical pulsation of fluids or device [1–5], electroosmotic forces [6–11], electrorheological control fluids [12], other electrokinetic forces [13–16], magnetic forces or beads [17–20], and acoustic vibration [21–23]. Many experimental [1,3–5,7,10–15,18,20–23], numerical [2,4,5,8,10,11,13,15,18–20,22], and theoretical [24–26] studies based on such techniques have appeared recently. A collection of review articles on microfluidic mixing devices appears in a dedicated supplement Ref. [27].

A common theme in recent experimental and numerical investigations is to time-periodically vary the force or velocity in the active strategy used (i.e., electrokinetic forcing, magnetic force field, pulsating fluid at inlet) [1–5,7–15,17–23,26,28]. While ac currents are a practical reason for this, a likely motivation is the concept of chaotic mixing [29]. Such a time-periodic strategy typically causes the fluid interface to split into stable and unstable manifolds, whose infinitely many intersections lead to complicated lobe dynamics [30,31]. Rom-Kedar and Poje [32] argue the presence of an optimum frequency at which cross-interface flux is maximum. Increasing the frequency leads to smaller lobe areas, but with quicker mixing between them, underlying the competition between the fluid areas which participate in mixing, and the speed of such mixing [32]. Under appropriate device geometries, the cross-interface flux is the mechanism through which chaotic mixing between the reagent and sample may be achieved [33].

For a particular flow geometry and mixing strategy, the mixing achieved as a function of the frequency has recently been an intensive area of study. There is strong experimental [5,7,10,11,13,14,18,20,21] and numerical [5,10,12,13,18] evidence for the presence of an optimum

frequency (or Strouhal number), usually obtained by laboriously testing many frequency values. In contrast, there are a few studies which either indicate that the mixing increases [3,4,9] or decreases [8,12] with frequency [35]. If an optimum frequency exists, there is no current insight or theory on how to find it.

This study focuses on determining such an optimal frequency, associated specifically with the cross-interface mixing [25,32,36,37] as opposed to other mixing measures [38]. It is the first theoretical tool available in optimum frequency analysis, and is easily computable using Fourier transforms. Two examples (loosely associated with an electromagnetic switching, and a side channel pumping situation) are presented. This new method could easily be used for different geometries and mixing strategies, providing a significant tool in the currently *ad hoc* process of designing micromixers.

*Optimal frequency determination.*—Consider a fluid interface in the nonmixing flow

$$\dot{x} = \frac{\partial H}{\partial y}; \quad \dot{y} = -\frac{\partial H}{\partial x}, \quad (1)$$

in which  $H(x, y)$  is the stream function (Hamiltonian). This incompressible steady laminar flow is assumed to possess fixed points  $\mathbf{a}$  and  $\mathbf{b}$  which are connected together by a heteroclinic trajectory  $\Gamma$ , which is simultaneously a branch of  $\mathbf{a}$ 's unstable manifold and  $\mathbf{b}$ 's stable manifold. The interface  $\Gamma$  can be represented by a solution  $[\bar{x}(t), \bar{y}(t)]$  of (1) which goes to  $\mathbf{a}$  as  $t \rightarrow -\infty$  and  $\mathbf{b}$  as  $t \rightarrow \infty$ . Mixing is induced across  $\Gamma$  (and thus between the fluids lying on either side of  $\Gamma$ ) via a time-dependent velocity in the form

$$\begin{aligned} \dot{x} &= \frac{\partial H}{\partial y} + \epsilon h_x(x, y) \cos \omega t; \\ \dot{y} &= -\frac{\partial H}{\partial x} + \epsilon h_y(x, y) \cos \omega t, \end{aligned} \quad (2)$$

in which  $\omega > 0$  is the frequency of perturbation,  $\epsilon$  is a small parameter, and  $\mathbf{h} = (h_x, h_y)$  is the spatial part of the perturbing velocity arising from whichever mixing strategy is being used [39].

The area of fluid per unit time crossing  $\Gamma$  near a position  $[\bar{x}(p), \bar{y}(p)]$  in the direction of  $\nabla H$  at a time instance  $t$  can

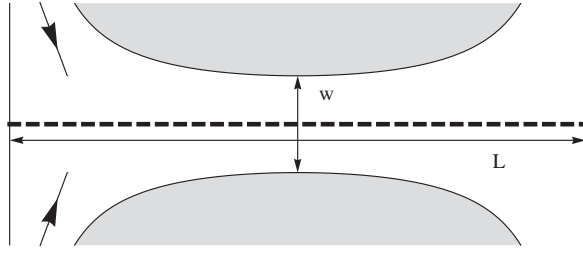


FIG. 1. Mixer geometry before a mixing strategy is employed.

be defined as the instantaneous flux [40], whose  $\mathcal{O}(\epsilon)$  term is given by the Melnikov function [42]

$$M(p, t) = |\Lambda(\omega)| \cos\{\omega(t - p) - \arg[\Lambda(\omega)]\}. \quad (3)$$

Here,  $\Lambda(\omega) := \mathcal{F}\{\lambda(t)\} = \int_{-\infty}^{\infty} \lambda(t)e^{-i\omega t} dt$  is the Fourier transform of

$$\lambda(t) := \nabla H[\bar{x}(t), \bar{y}(t)] \cdot \mathbf{h}[\bar{x}(t), \bar{y}(t)]. \quad (4)$$

The Melnikov-flux expression (3) predicts fluid sloshing back and forth across  $\Gamma$  for nonzero frequencies if  $\Lambda(\omega) \neq 0$  [44]. The average flux quantifies the area of lobes crossing  $\Gamma$  per unit time [30], and is given by [45]

$$s(\omega) = \epsilon \frac{2}{\pi} |\Lambda(\omega)| + \mathcal{O}(\epsilon^2). \quad (5)$$

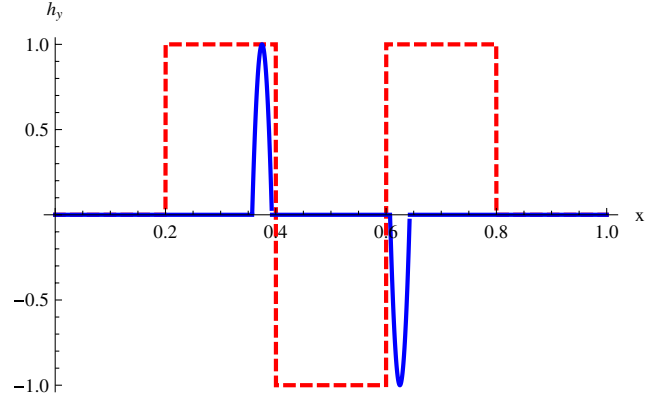
The fact that the flux decays to zero as  $\omega \rightarrow \infty$  is immediately captured by (5) [46]. This provides a tool to find the optimal frequency for a given flow geometry by numerically investigating the Fourier transform of  $\lambda(t)$  [48]. Frequencies which either maximize or minimize the flux can also be shown to obey the fact that  $\Lambda(\omega)$  and  $\Xi(\omega) = \mathcal{F}\{t\lambda(t)\}$  lie on the same two-sided ray through the origin in the complex plane [49], that is

$$\arg[\Lambda(\omega)] = \arg[\Xi(\omega)] + n\pi, \quad n \text{ an integer}. \quad (6)$$

*An electromagnetic example.*—To replicate the common “*T*-mixer” inlet geometry [1,7,10,11,15], and to provide an easy illustrative situation, consider  $H(x, y) = ax(L - x)y$ . The flow is

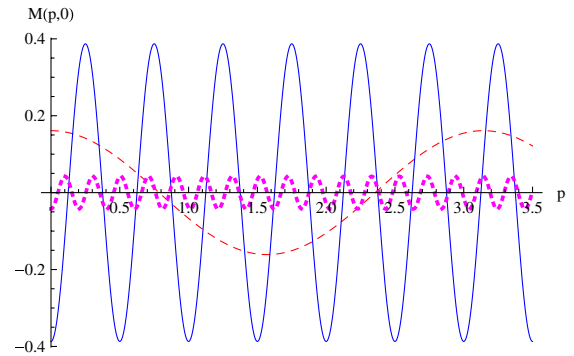
$$\dot{x} = ax(L - x); \quad \dot{y} = -ay(L - 2x)$$

in the channel  $0 < x < L$ , with sides  $|y| < wL^2/[8x(L - x)]$ , as shown in Fig. 1. The two fluids coming from opposite directions near the left inlet do not mix across the dashed fluid interface  $[\bar{x}(t), \bar{y}(t)]$  which connects the points  $(0,0)$  and  $(L, 0)$ , and which is given by  $\bar{x}(t) = L/(1 + e^{-aLt})$ ,  $\bar{y}(t) = 0$  [50]. Suppose three electromagnetic plates are located outside the channel in the locations  $L/5 < x < 2L/5$ ,  $2L/5 < x < 3L/5$ , and  $3L/5 < x < 4L/5$  and switched out of phase with the adjacent plates, in order to induce the (ac-modulated) transverse velocity  $h_y(x, 0)$  as given in Fig. 2 by the dashed curve [51]. Figure 3 shows (3) at three different frequencies, and represents the topological intersection pattern between

FIG. 2 (color online). Transverse velocity  $h_y(x, 0)$  for electromagnetic (dashed) and fluid pumping (solid) strategies with  $L = 1$ .

perturbed stable and unstable manifolds. Figure 4 shows the leading-order average flux of (5). Larger  $\omega$  values (not shown) have smaller and smaller humps similar to those displayed [52]. The mixing optimizing frequency is, from Fig. 4, approximately  $\bar{\omega} = 4\pi$ , which corresponds to the solid curve in Fig. 3. Since  $\Lambda(\omega)$  is real and  $\Xi(\bar{\omega})$  is imaginary in this situation, (6) is satisfied by  $\Xi(\bar{\omega}) = 0$  [53].

*A fluid pumping example.*—Retain the base (laminar) *T*-mixer structure of the previous example, but adopt a different mixing strategy. Suppose now that there are two side channels in which fluid is sloshed into the main channel. Mimicking the dimensions of the experimental syringe-pump ultrashort micromixer of Bottausci *et al.* [4] as closely as possible, this corresponds to choosing  $h_y(x, y)$  as in the solid curve in Fig. 2, once again independent of  $y$ . A parabolic profile normalized with a maximum speed of unity has been fitted to the two side channels centered at  $x = 21L/56$  and  $35L/56$ , each with width  $L/28$  [54]. The profile in the side channels is also motivated by the results of Niu *et al.* [12], who used particle tracking in an electrorheologically controlled microchip to experimen-

FIG. 3 (color online). Melnikov function at  $t = 0$  using the electromagnetic strategy, with  $a = 4$  and  $L = 1$ :  $\omega = 2$  (dashed),  $\omega = 4\pi$  (solid), and  $\omega = 31$  (dotted).

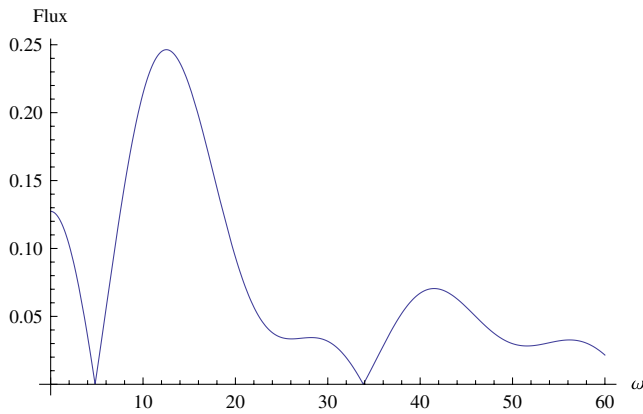


FIG. 4 (color online). Leading-order average flux: electromagnetic strategy.

tally obtain a parabolic profile modulated by  $\cos\omega t$ , exactly as postulated here. Once again, the optimum frequency is around  $\bar{\omega} = 4\pi$ , as is clear from Fig. 5, and (6) is satisfied in a degenerate sense with  $\Xi(\bar{\omega}) = 0$  [55]. Note the existence of much larger frequencies (e.g.,  $\omega = 38, 62$ ) which also produce relatively high mixing.

*Concluding remarks.*—The theoretical tool presented here is useful in determining best frequencies for a time-periodic mixing strategy, in order to specifically increase mixing across the fluid interface between the sample and reagent. The limitations are that the theory cannot be applied to maximize global mixing measures, or to situations in which the time-periodic flow is not secondary. Nevertheless, it is a significant analytical tool in a research area in which such tools are lacking, and may well provide a good initial guess for the optimum frequency when these conditions are not met. Given a particular dominant flow geometry and knowing the cross-interface fluid velocity resulting from a mixing strategy, the Fourier transform expressions (5) and (6) provide easy tools for analysis of the optimum frequency, using fast-Fourier-transform software as needed. The formulation provides additional in-

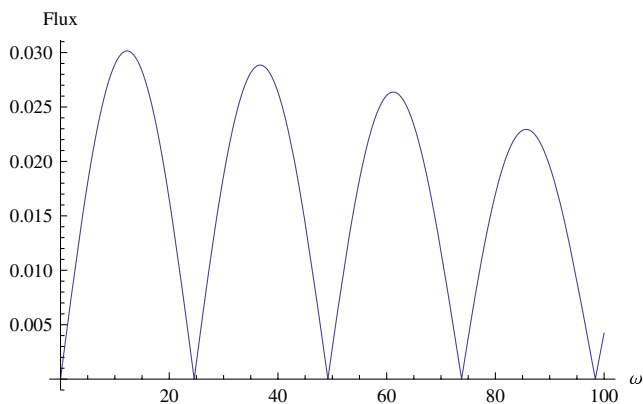


FIG. 5 (color online). Leading-order average flux for fluid pumping.

sights: the eventual decay to zero of mixing as the frequency gets larger, the potential for arbitrarily small frequencies to be flux maximizing [56], and the prediction of nonoptimum frequencies [Fig. 5, for example, shows that using frequencies like  $\omega \approx 24$  or 48—also captured by (6)—lead to diminished mixing]. The significant difficulties in obtaining each data point in experimental design of micromixers can be ameliorated by judicious use of this tool.

\*Also at Department of Mathematics, Connecticut College, New London, CT 06320, USA.

sanjeevabalasuriya@yahoo.com

- [1] I. Glasgow and N. Aubry, *Lab Chip* **3**, 114 (2003).
- [2] X. Niu and Y.-K. Lee, *J. Micromech. Microeng.* **13**, 454 (2003).
- [3] N. Reis, A. Vicente, J. Teixeira, and M. Mackley, *Chem. Eng. Sci.* **59**, 4967 (2004).
- [4] F. Bottausci, C. Cardonne, C. Meinhart, and I. Mezić, *Lab Chip* **7**, 396 (2007).
- [5] A. Rodrigo, R. Rodrigues, N. Formiga, and J. Mota, *Chem. Eng. Commun.* **193**, 743 (2006).
- [6] S. Qian and H. Bau, *Anal. Chem.* **74**, 3616 (2002).
- [7] C. Lim, Y. Lam, and C. Yang, *Biomicrofluidics* **4**, 014101 (2010).
- [8] H. Sugioka, *Phys. Rev. E* **81**, 036306 (2010).
- [9] W. Ng, S. Goh, Y. Lam, C. Yang, and I. Rodríguez, *Lab Chip* **9**, 802 (2009).
- [10] C.-H. Lin, L.-M. Fu, and Y.-S. Chien, *Anal. Chem.* **76**, 5265 (2004).
- [11] H. Song, Z. Cai, H. Noh, and D. Bennett, *Lab Chip* **10**, 734 (2010).
- [12] X. Niu, L. Liu, W. Wen, and P. Sheng, *Appl. Phys. Lett.* **88**, 153508 (2006).
- [13] L.-M. Fu, R.-J. Yang, C.-H. Lin, and Y.-S. Chien, *Electrophoresis* **26**, 1814 (2005).
- [14] S. Shin, I. Kang, and Y.-K. Cho, *J. Micromech. Microeng.* **15**, 455 (2005).
- [15] D. Yan, C. Yang, J. Miao, Y. Lam, and X. Huang, *Electrophoresis* **30**, 3144 (2009).
- [16] C.-C. Chang and R.-J. Yang, *Microfluid. Nanofluid.* **3**, 501 (2007).
- [17] M. Yi, S. Qian, and H. Bau, *J. Fluid Mech.* **468**, 153 (2002).
- [18] Y. Wang, J. Zhe, B. Chung, and P. Dutta, *Microfluid. Nanofluid.* **4**, 375 (2008).
- [19] T. Le, Y. Suh, and S. Kang, *J. Mech. Sci. Tech.* **24**, 441 (2010).
- [20] H. Suzuki, C.-M. Ho, and N. Kasagi, *J. Microelectromech. Syst.* **13**, 779 (2004).
- [21] S. Wang, Z. Jiao, X. Huang, C. Yang, and N. Nguyen, *Microfluid. Nanofluid.* **6**, 847 (2009).
- [22] M. Tan, L. Yeo, and J. Friend, *Europhys. Lett.* **87**, 47003 (2009).
- [23] S. Oberti, A. Neild, and T. Ng, *Lab Chip* **9**, 1435 (2009).
- [24] S. Balasuriya, *Phys. Fluids* **17**, 118103 (2005).
- [25] S. Balasuriya, *Physica (Amsterdam)* **202D**, 155 (2005).
- [26] A. Vikhansky, *Phys. Fluids* **14**, 2752 (2002).

- [27] R. Daw and J. Finkelstein, *Nature (London)* **442**, 367 (2006).
- [28] T.H. Solomon, S. Tomas, and J.L. Warner, *Phys. Rev. Lett.* **77**, 2682 (1996).
- [29] Special issue on Chaotic Mixing in Relation to Microfluidic Devices, edited by J.M. Ottino and S.R. Wiggins [*Phil. Trans. R. Soc. A* **362**, 923 (2004)].
- [30] V. Rom-Kedar, A. Leonard, and S. Wiggins, *J. Fluid Mech.* **214**, 347 (1990).
- [31] S. Wiggins, *Chaotic Transport in Dynamical Systems* (Springer-Verlag, New York, 1992).
- [32] V. Rom-Kedar and A.C. Poje, *Phys. Fluids* **11**, 2044 (1999).
- [33] The infinitely many lobes along the interface become increasingly elongated when approaching the end points; device geometry usually constrains these elongated lobes to reentrench into the mixing region, resulting in chaotic mixing via the Smale-Birkhoff theorem [34].
- [34] J. Guckenheimer and P. Holmes, *Nonlinear Oscillations, Dynamical Systems and Bifurcations of Vector Fields* (Springer, New York, 1983).
- [35] The monotonic relationship between the flux and frequency claimed in several experimental studies [3,4,8,9,12] may well arise in sampling a nonmonotonic function in a monotonic region.
- [36] S. Balasuriya, *SIAM J. Appl. Dyn. Syst.* **4**, 282 (2005).
- [37] S. Balasuriya, *Nonlinearity* **19**, 2775 (2006).
- [38] For example Lyapunov exponents [2,20], concentration or intensity variances [1,4,5,7,9–11,14,18,19,21] or stirring times [8].
- [39] While an optimal frequency exists under quite general conditions [32], the current theory requires small  $\epsilon$  and finite (but nonzero)  $\omega$ . The asymptotic limits of small and large  $\omega$ —not covered here—is also known [32].
- [40] Defining this relates to taking time-dependent perturbed manifolds and a gate between them as suggested by Haller and Poje [41]; see Balasuriya [37] for details.
- [41] G. Haller and A. Poje, *Physica (Amsterdam)* **119D**, 352 (1998).
- [42] Modifying standard results [31,34] using a forward-parametrization of the heteroclinic [43], a time-dependent flux [37], and ideas presented in a slightly different context [24,25,36] give  $M(p, t) = \int_{-\infty}^{\infty} \lambda(\tau) \cos[\omega(\tau + t - p)] d\tau$ . Expanding  $\cos[\omega(\tau + t - p)] = \cos\omega(t - p) \times \cos\omega\tau - \sin\omega(t - p) \sin\omega\tau$ , pulling out  $\tau$ -independent terms, and multiplying and dividing by  $|\Lambda(\omega)|$  yields (3).
- [43] S. Balasuriya and G. Gottwald, *J. Math. Biol.* **61**, 377 (2010).
- [44] Flux arises for any  $\omega > 0$  if  $\Lambda(\omega) \neq 0$ , since  $M(p, t)$ 's relation to the  $p$  axis is topologically equivalent to the intersection pattern between perturbed stable and unstable manifolds at a time instance  $t$ , and the form (3) leads to infinitely many intersections.
- [45] By shifting the periodic integral to convenient locations  $\frac{\omega}{2\pi} \int_0^{2\pi/\omega} |M(p, t)| dt = |\Lambda(\omega)| \frac{\omega}{2\pi} \int_0^{2\pi/\omega} |\cos\omega t| dt = |\Lambda(\omega)| \frac{2\omega}{\pi} \int_0^{\pi/(2\omega)} \cos\omega t dt$ , giving the desired result which is independent of  $p$  [25,36].
- [46] The amplitude of classical Fourier transforms goes to zero as  $\omega \rightarrow \infty$  by the Riemann-Lebesgue lemma ([47], e.g.).
- [47] R.S. Strichartz, *A Guide to Distribution Theory and Fourier Transforms*, Studies in Advanced Mathematics (CRC Press, Boca Raton, Florida, 1994).
- [48] While the  $t$  parametrization on  $\Gamma$  is only unique up to a shift, using a different parametrization  $t \rightarrow t - \tau$  has no effect on the average flux, since  $\Lambda(\omega)$  would simply be multiplied by  $e^{i\omega\tau}$ , which does not modify its modulus.
- [49] Set the derivative of  $|\Lambda(\omega)|^2 = [\int_{-\infty}^{\infty} \lambda(t) \cos(\omega t) dt]^2 + [\int_{-\infty}^{\infty} \lambda(t) \sin(\omega t) dt]^2$  equal to zero, and rearrange to obtain that  $\text{Re}[\Lambda(\omega)]/\text{Im}[\Lambda(\omega)]$  is identical to the similar expression for  $\Xi(\omega)$ .
- [50] For lobe dynamics, a stable and unstable manifold must intermingle. This stream function ensures a stable manifold associated with a fixed point near the outlet.
- [51] By (4),  $h_x$  causes no leading-order mixing.
- [52] Note the limit  $\omega \rightarrow 0$  leads to a constant Melnikov function, associated with the perturbed stable and unstable manifolds not intersecting if  $\Lambda(0) \neq 0$ , leading to a non-mixing unidirectional flow across  $\Gamma$ .
- [53] The flux-minimizing frequencies ( $\omega \approx 4.8, 34, \dots$ ) are also captured by (6); since  $\Xi$  is imaginary,  $\Lambda$  must be zero.
- [54] The length  $L$  of Bottausci *et al*'s [4] micromixer is about 1400  $\mu\text{m}$ , and side channels have width about 1/28th of this. The width of their main channel (about 200  $\mu\text{m}$ ) is irrelevant here, with only transverse velocity information on the separating interface needed.
- [55] This is the reverse of the electromagnetic example, and has  $\Lambda$  imaginary and  $\Xi$  real. The symmetry of the heteroclinic time parametrization and the (anti)symmetry of the perturbation leads to this nice behavior.
- [56] If  $\Lambda(0)^+ \neq 0$  as in Fig. 4 and if  $|\Lambda(\omega)| \leq |\Lambda(0)^+|$ , then the smaller the frequency, the larger the mixing.